PRE-PRINT OF MANUSCRIPT SUBMITTED TO QUARTERLY JOURNAL OF THE ROYAL METEOROLOGICAL SOCIETY

Moist Convection and Radiative Cooling: Dynamical Response and Scaling

Lokahith Agasthya[1] | Caroline Muller[1]

[1]Institute of Science and Technology Austria, Am Campus 1, 3400 Klosterneuburg, Austria

[2]École Normale Supérieure de Lyon, 15 parvis René Descartes, BP 7000, 69342 Lyon Cedex 07, France

Correspondence
Lokahith Agasthya, Institute of Science and Technology Austria, Am Campus 1, 3400 Klosterneuburg, Austria
Email: lnagasthya@gmail.com

Present address
Institute of Science and Technology Austria, Am Campus 1, 3400 Klosterneuburg, Austria

Funding information
European Union Horizon 2020 research and innovation programme, Marie Sklodowska-Curie grant agreement No. 101034413; European Research Council (ERC), European Union Horizon 2020 research and innovation programme, Project CLUSTER, Grant Agreement No. 805041

Moist convection is a fundamental process occurring in the Earth's atmosphere. It plays a central role in the weather and climate of the tropics where, to first order, the heating of the atmosphere by convection is in balance with the cooling of the atmosphere by the emission of radiation to outer space. In this study, we use a Cloud Resolving Model in Radiative-Convective Equilibrium with an imposed constant rate of radiative cooling and study the response of moist convection to varying this rate of radiative cooling. We recover the previously known result that in response to increasing radiative cooling, the area of convection expands rapidly while the intensity of convection does not change. We explore the robustness of this response under varying model parameters and find that this response is due to a combination of moist convective processes and changes in the boundary layer. We also propose a fundamental scaling of the non-dimensional cumulus mass flux in moist convection which is robust across models of different complexity. We aim to bridge the gap between highly idealised prototypes of moist convection such as "Rainy-Bénard convection" introduced by Vallis et al. (2019) and comprehensive cloud-resolving models.

KEYWORDS
Moist Convection, Radiative Cooling

1 | INTRODUCTION

Convection is an overturning circulation of a fluid (Rayleigh, 1916) driven by vertical differences in density where denser fluid falls vertically downward while lighter fluid is lifted vertically upward. In the atmosphere (Emanuel, 1994), convective circulations are usually driven by local heating from the Earth's surface, which leads to the layer of air in contact with the surface to be lighter than the air above it, thus rising and bringing colder air from aloft to the surface through a compensating subsidence. Convection is a leading driver of heat and moisture transport in the Earth system and it is particularly important in the tropics, where deep, moist convection plays a dominant role in determining tropical weather and climate. Convection occurs either in isolated thunderstorms, as part of broader systems (Mesoscale Convection Systems, Monsoons) or in conjunction with other synoptic and planetary scale phenomena, such as Equatorial Waves, the Madden-Julien Oscillations, or the Hadley Cell (Houze Jr., 2004; Stevens, 2005; Kiladis et al., 2009; Zhang, 2005).

The Earth's atmosphere loses heat to outer space by (chiefly longwave) radiation (Manabe and Strickler, 1964; Jeevanjee and Fueglistaler, 2020). In the tropics, the leading order energy balance is between radiative cooling and the warming of the troposphere by convection, or radiative-convective equilibrium (RCE) (Tompkins and Craig, 1998). RCE holds over large enough length and time scales in the tropics (Muller and O'Gorman, 2011; Jakob et al., 2019) and is a key lens used to understand tropical dynamics. Studies of RCE use limited-domain cloud-resolving models (CRMs) where, without large-scale forcing in the steady-state, radiation and convection are in equilibrium. CRMs have proved a valuable tool in gaining insight and understanding into several aspects of moist convection and tropical dynamics (Wing and Emanuel, 2014; Stauffer and Wing, 2022), especially the changes in tropical climate in a global warming scenario characterised by higher surface temperatures (Muller et al., 2011; Singh and O'Gorman, 2015). Behaviour observed in CRMs have instigated studies into realistic models and observations (Holloway et al., 2017; Wing et al., 2017). The utility of CRMs however goes well beyond mean-state tropical dynamics. CRMs can be used in non-RCE configurations with the boundary conditions and energetic and mass-balances configured to mimic real-world conditions and the influence from large-scales onto limited area models (Singh and Neogi, 2022).

Convection warms the atmosphere by transporting heat upwards, mainly by the transport of water vapour (or latent heat) which condenses (and freezes) aloft in the atmosphere. The convective transport of latent heat occurs via rising cloud plumes in which the air is saturated with moisture. The dynamics of these plumes is set by complex, non-linear mutually interacting cloud processes involving both, the large-scale conditions as well as the microphysics of water condensates (Arakawa and Schubert, 1974; Arakawa and Wu, 2013). A commonly used measure for the strength of convection is the rate of upward transport of air within cloud-plumes, or the cloudy mass-flux (known henceforth as simply the mass-flux). Under RCE, the greater the radiative cooling, the greater the mass-flux. The mass-flux M_c at a given height can be written as

$$M_c = \rho \sigma w_c \tag{1}$$

where ρ is the density of dry air, σ_c is the area-fraction of the horizontal cross-section that is occupied by clouds and w_c is the typical vertical velocity within these clouds.

The scaling of the mass-flux with changes in radiative cooling has been previously studied in CRMs (Robe and Emanuel, 1996) (see also similar simulations by Cohen and Craig (2006)), where it was found that while M_c increased strongly with the imposed rate of radiative cooling R, this increase occurred by an increase in the area of clouds (ie., increase in σ) while the intensity of updrafts in the clouds (ie., w_c) remained nearly constant. This scaling has also been observed in other numerical simulations, for example in Shutts and Gray (1999) (see Figures 7, 8 and Table 1), and

Parodi and Emanuel (2009) (see Figure 8 showing updraft velocity for large changes in the radiative cooling). Further, the dynamic consequences of the expanding area of convection and constant vertical velocity in clouds in response to increase radiative cooling are reviewed in Yano and Plant (2012). More recently, the response of dry and moist convection to varying rates of bulk cooling was studied in idealised 2D Direct Numerical Simulations (Agasthya and Muller, 2024; Agasthya et al., 2025). In Agasthya et al. (2025) (henceforth AMC25), using the Rainy-Bénard model of moist-convection (Vallis et al., 2019) the study found that the same scaling in response to radiative cooling holds even in highly idealised, 2D settings, establishing that this scaling is a fundamental feature of moist convection and not the consequence of parametrised sub-grid scale processes or not set by the microphysics of liquid water and ice.

In this study, we revisit the simulations of Robe and Emanuel (1996) (henceforth RE96) and study the scaling of moist convection in the light of several new findings around moist convection in the intervening time of three decades. In addition to changing the mass-flux, increased radiative cooling affects domain-mean temperatures, with more cooling leading to a colder domain. Here, we decouple the changes in the dynamics due to the changing temperature of the domain from the changes due to the altered circulation caused by varying radiative cooling. Further, we use the fundamental insights gained from idealised models to understand changes in cloudy area, arguing that fundamental constraints from convective dynamics and the changes in the boundary layer lie at the heart of the wide-spread convection seen in simulations with large radiative cooling. Finally, we identify that the average velocity in clouds is a fundamental velocity scale. Using this velocity scale, we show that in idealised moist convection, a simple power-law scaling exists between the non-dimensionalised mass-flux and the non-dimenionsalised ratio of radiative cooling to condensation heating.

The rest of the article is organised as follows. § 2 details the cloud resolving model used for our RCE studies and the numerical experiments performed. § 3 outlines the main results and scientific insights gained from these simulations. In § 4, we summarise our work and point to potential future avenues of research.

2 | METHODOLOGY

We perform RCE simulations using the System for Atmospheric Modeling (SAM) (Khairoutdinov and Randall, 2003) version 6.10.8. SAM uses anelastic momentum and scalar advection-diffusion equations with prognostic thermodynamic equations for liquid water/ice static energy, total precipitating water, and total non-precipitating water. Microphysical processes are parameterized using 1-moment microphysics while subgrid scale turbulence closure is parameterized using a Smagorinsky-type parameterization (as in Bretherton et al., 2005; Muller and Held, 2012). Surface fluxes are parameterized using bulk formulas based on Monin–Obukhov similarity. The equations are solved on a 128 km×128 km horizontally periodic square domain with horizontal grid-spacing of 1 km. The domain is 27 km high, with a sponge layer with Newtonian damping on all prognostic variables to absorb gravity-waves in the top 9 km. There are a total of 64 vertical levels, with 53 in the first 18 km including 9 levels in the lowest 1 km. The lowest atmospheric model level is at 37.5 m and the vertical resolution decreases with height to 400 m in the mid and upper troposphere. A constant radiative cooling rate $-R$ K d^{-1} is imposed up to a height of 10 km above which it is gradually relaxed to 0 at a height of 14 km. For temperature colder than 200 K, we applying a Newtonian damping to this temperature with a timescale of 2 days. This leads to a uniform cooling in most of the troposphere while maintaining stratospheric temperatures close to 200 K (similar to Pauluis and Garner (2006)).

The first set of 5 simulations are performed with an SST of 300 K and the magnitude of the imposed radiative cooling R varying from 0.75 K d^{-1} to 7.2 K d^{-1}. In-line with expectations and RE96, we find that the average air temperature in the domain decreases in response to a stronger cooling. Thus, any changes when R is increased could

	Varying Air Temperature (VAT)				Tuned Air Temperature (CAT)			
R	SST	T_a	SHF	LHF	SST	T_a	SHF	LHF
0.75	300	297.98	6.41	66.62	296.8	294.35	7.66	61.03
1.5	300	294.56	20.82	118.73	300	294.56	20.82	118.73
2.0	300	292.28	31.89	149.11	302	294.88	29.75	160.85
3.6	300	286.71	72.97	240.29	305.8	294.16	53.91	285.40
7.2	300	279.91	165.06	401.20	312.5	293.90	109.82	579.46

TABLE 1 The imposed value of R ($\mathrm{K\,d^{-1}}$) and SST (K) for the VAT and CAT simulations. The various averaged quantities shown are respectively the lowest atmospheric level temperature T_a (K), surface Sensible Heat Flux SHF, and surface Latent Heat Flux LHF (both in $\mathrm{W\,m^{-2}}$).

be due to changes in the circulation due to the direct effect of R or could be an indirect effect of the change in the air temperature. To isolate the former dynamic responses from the latter thermodynamic response, we perform an additional set of simulations where the SST is tuned by having a larger SST for simulations with larger R. This SST tuning ensures that the temperature of the lowest atmospheric level in the model T_a is within less than 1 K of that in the simulation with SST of 300 K and $R = 1.5\,\mathrm{K\,d^{-1}}$. This tuning leads to the average air temperature profile to be nearly identical across the simulations with different R. Henceforth, the first set of simulations with SST of 300 K and varying R will be known as the varying air temperature, or VAT, simulations. The second set of simulations with SST tuned such that the air temperatures are identical will be known as constant air temperature, or CAT simulations. The reader must note that the simulation with SST = 300 K and $R = 1.5\,\mathrm{K\,d^{-1}}$ is common to VAT and CAT and is henceforth referred to as control simulation (CTRL). All simulations are run until they reach a steady-state and all analysis is performed after that transient period using 50 days of steady-state dynamics.

3 | RESULTS

3.1 | Response of temperature, moisture and mass-flux

The imposed SST and various important simulation quantities are summarized in Table 1. For the VAT simulations, T_a shows a sharp decrease with increasing R as the domain gets colder. The surface heat fluxes increase rapidly to balance the cooling in the domain, with the sensible heat showing a much larger relative increase than the latent heat. This can be attributed to the fact that sensible heat becomes more important as the domain becomes drier. As noted in § 2, the CAT simulations have different SSTs but the resulting T_a are nearly the same, within < 1 K of each other. For larger R, the CAT simulation domains have nearly identical temperature and moisture as CTRL. We also note that the surface fluxes (SHF + LHF) are stronger in the large R CAT simulations due to the increased convection depth in a warmer domain, leading to a higher stratosphere and thus, stronger vertically integrated radiative cooling that needs to be balanced by stronger incoming surface fluxes.

The time-averaged vertical profiles of temperature T, water-vapour mixing ratio q_v and relative humidity are shown in Figure 1. In the VAT simulations (top panels of Figure 1), for increasing R (darker shades of blue), the temperature in the domain decreases significantly, also leading to a decrease in q_v as well as large variations in the relative humidity profiles. We note in passing that the profiles shrink vertically with cooling, consistent with previous work (Singh and O'Gorman, 2012). The profiles show consistency when plotted using temperature as a vertical coordinate (Jeevanjee, 2022) (also see Appendix A), a theme that we will return to later.

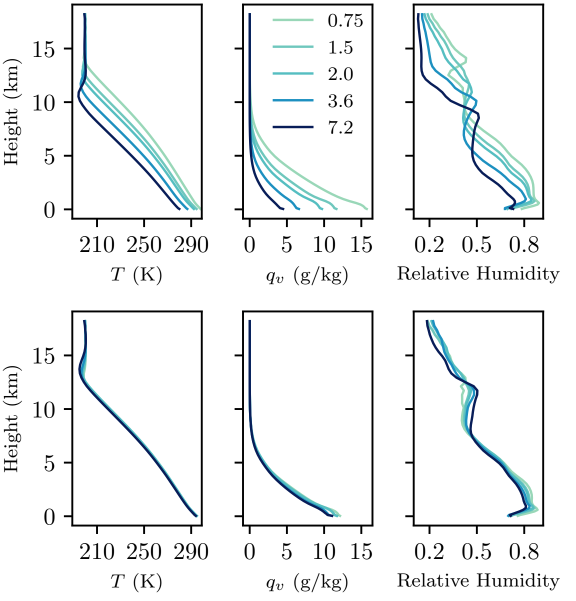

FIGURE 1 (From left to right) Horizontal and time-average profiles of Temperature, water vapour mixing ratio and relative humidity for the 5 values of R (values shown in legend with units K d^{-1}) with VAT (top panels) and CAT (bottom panels).

For CAT simulations, we see that not only the lowest model level temperature but the temperature profiles of all the simulation domains are very close to each other and are nearly indistinguishable from each other in the plotted figure. Though temperature differences of the order of 2 K are present, this is a first indication that the temperature profile, which is in turn set by convection, is a function of surface temperature and moisture, independent of the radiative cooling.

As discussed in RE96 and AMC25, greater radiative cooling leads to an increase in the magnitude of the average subsiding vertical velocity w_{sub} outside clouds. This subsidence is radiatively driven and the subsidence adiabatic warming plays an important role in balancing the imposed cooling. From the conservation of mass, w_{sub} is related to the cloud mass-flux at a given height as

$$M_c = \overline{\rho}\sigma w_c = \overline{\rho}(1-\sigma)|w_{sub}|, \quad (2)$$

where the line over ρ indicates that it is the anelastic density profile which is a function of height alone. Here w_{sub} is the vertical velocity averaged only over regions that are not clouds while w_c and σ are the vertical velocity averaged within clouds and the area fraction of clouds respectively. Away from clouds, assuming a balance between radiative cooling and subsidence warming yields (e.g. Robe and Emanuel (1996))

$$w_{sub} = \frac{-R}{\frac{T}{\theta}\partial_z\theta} \equiv \frac{-R}{S} \quad (3)$$

where θ is the potential temperature and S is known as the dry stability of the column, which is proportional to the difference between the dry and moist adiabatic lapse rates (Bony et al., 2016; Jeevanjee, 2022). This suggests that, up to changes in stability (which can be significant), the subsidence velocity must scale proportionally with the radiative cooling.

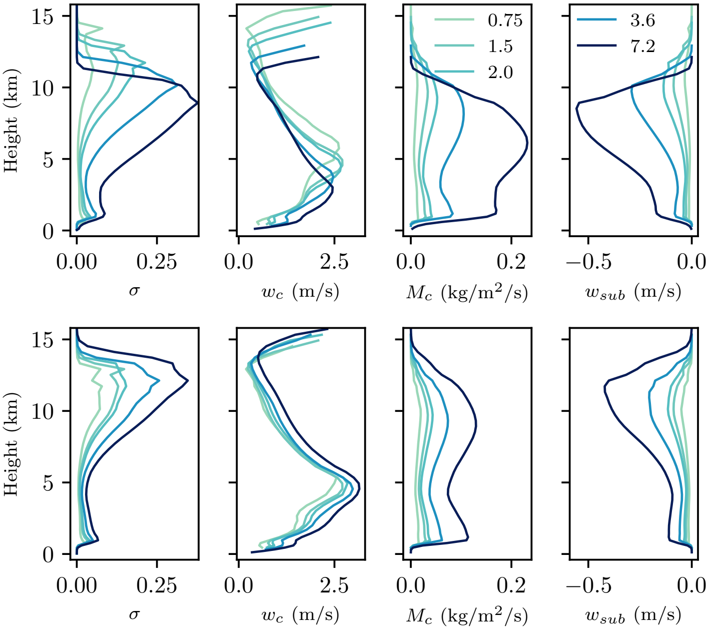

FIGURE 2 (From left to right) Time and horizontally averaged profiles of cloudy area fraction, average vertical velocity in clouds, cloudy mass flux and average vertical velocity outside clouds for (top panels) varying air temperature and (bottom panels) tuned air temperature simulations. A grid-point is considered to be cloudy is the mixing ratio of non-precipitating water (cloud water + cloud ice) $q_n > 10^{-5}$ g/kg and $w > 0$.

Henceforth in our analysis, we define a grid-point to be "cloud" if it is rising ($w > 0$) and has a non-precipitating condensate mixing ratio q_n greater than 10^{-5} kg/kg, a fairly standard definition of a cloud in the literature. Figure 2 shows the time-and-horizontally averaged profiles of σ, w_c, M_c and w_{sub}. In the top panels showing the averages of the VAT simulations, we recover the result that while the mass-flux increases rapidly with stronger radiative cooling, w_c remains fairly constant, showing a mid-tropospheric maximum that is insensitive to R. The increase in the mass-flux is driven by the large increase of σ – the mass-flux increases by having more clouds with the same intensity of convection. On the flip-side, w_{sub} also shows a large increase with increasing R, closely mirroring the increase in mass-flux, as expected from (3). Here, S decreases for simulations with larger R as the domain becomes drier and the dynamics approach dry convection. It is important to note here that the convection becomes shallower for increasing R in the VAT simulations. This can be gauged either by observing the peaks of w_c and w_{sub} or by noticing that σ goes to 0 in the upper troposphere closer to $z = 14$ km for $R = 0.75\,\mathrm{K\,d^{-1}}$ while this happens closer to $z = 11$ km for $R = 7.2\,\mathrm{K\,d^{-1}}$. This becomes important, while comparing convective quantities at a given height, something we will come back to later.

The same profiles from the CAT simulations are shown in the lower panels of Figure 2. Here too, the increase in mass-flux with increasing R is pronounced and this increase is driven mainly by the increase in σ, an increase that is also seen in the magnitude of w_{sub}. However, w_c shows a small, monotonous increase at every height up to $\sim$ 12 km, and the highest value occurring at nearly the same height across the simulations. The maximum w_c shows a monotonic increase – however, the fractional increase in this peak is still small compared to the increase in R or σ – merely a $\sim$ 25% increase for a 9.6 times larger forcing (or 860% increase) and a 12.5 K warmer SST.

This is accompanied rather puzzlingly by a decrease of 80% and 18% in CAPE for VAT and CAT respectively. CAPE, short for convective available potential energy is a measure of the potential energy for convection in a given column of the atmosphere. It is defined as the positive part of the buoyancy of a moist-adiabatic parcel lifted from the surface and is known to be strongly associated with intense convective activity and thunderstorms (Johns and Doswell III, 1992). CAPE decreases in the VAT simulations because of a significant decrease in temperature and moisture available for convection, while in the CAT simulations, the decrease is due to small changes in the relative humidity and q_v in the domain (see lower middle and right panels of Figure 1). Thus, we see a decrease in CAPE but an overall increase in the average vertical velocity in clouds. Given that CAPE is usually associated with extreme events rather than average clouds, we also assess the extreme vertical velocity. The peak of the vertical profile of the 99.99-th %-ile w also shows a monotonic increase of 68% in CAT (not shown). For VAT, the increase from the simulation with the smallest R to the largest R is $\sim$ 32%, though this increase is not monotonic. Instead, the peak lies between 19 m/sec to 21.5 m/sec in all the simulations except the smallest R. It remains to be seen why despite a large increase in the surface forcing and a strengthening of the circulation with a strong subsidence flow, w_c increases by only a small amount, a change opposite in sign to the change in the moist instability as traditionally measured by CAPE.

3.2 | Relative changes in convective quantities

To understand the precise scaling of these quantities with the changes in radiative cooling, in the top panels of Figure 3 we plot their relative (or fractional) changes against the relative change in R for VAT (left) and CAT (right). The plots also have the black, dotted $y = x$ straight-line for reference, as a linear relationship would lie on this curve. The relative changes of the quantities w_c, σ, M_c, w_{sub} and R/S are plotted at a given temperature level rather than a chosen vertical height. While these quantities have been previously compared at a fixed height (for example a height of 6.7 km in RE96), we argue that the temperature level is a better way to ensure like-for-like comparisons (Jeevanjee, 2022). This is discussed further in Appendix A.

The scaling for the VAT case are nearly identical to the scaling seen in Figure 3(a) of AMC25, with the mass-flux (solid curve, crosses) increasing faster than R (a super linear increase), the area of convection (square markers) increasing linearly with R and the velocity within clouds showing very little change (dashed curve, circular markers). Outside clouds, the subsidence velocity (solid curve, triangles) scales similar to the predicted R/S scaling where S is calculated from the mean vertical temperature profile. In colder domains, S is smaller, leading to a super-linear increase of R/S with R. Given that the changes are measured at the same temperature level, a small part of the increase in M_c can also be attributed to the change in density, where for the simulations with larger R, the 250 K level is lower down in the domain and thus the density of air is also larger.

In the CAT simulations, all the domains have the 250 K level at the same height and thus the changes are purely due to the changes in the circulation and the convection which are the result of the changing R. Here the mass-flux increases slightly slower than linearly, exactly with w_{sub}. The increase of R/S on the other hand is slightly faster than linear, which is due to small changes in the stability with changing relative humidity and the fact that the temperature profiles are not exactly identical.

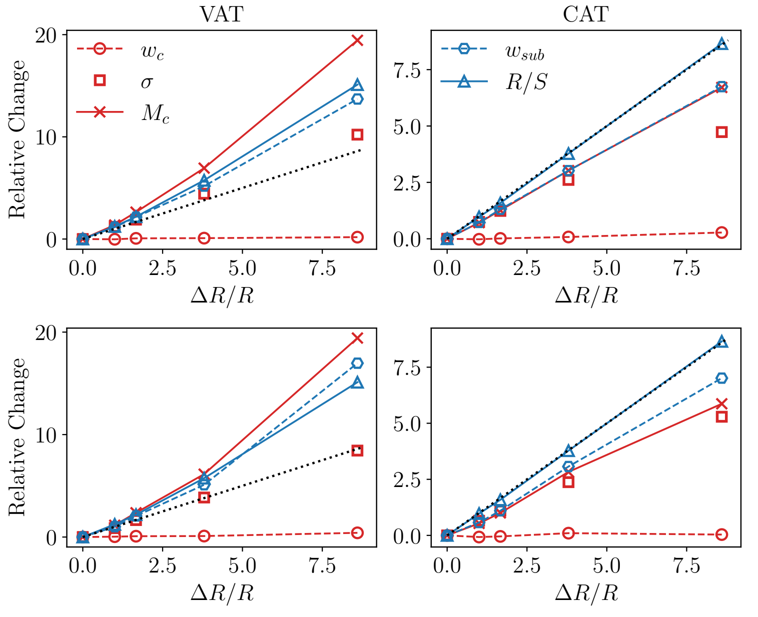

FIGURE 3 Relative change of various quantities in VAT (left) and CAT (right) simulations plotted against relative change in R linearly interpolated to the temperature level $T = 250$ K within each simulation (note the change in y-axis range across panels). This corresponds to ~ 6.5 km in CTRL and all CAT simulations, while it varies from 7.6 km to 3.8 km in VAT simulations. The relative changes plotted in the upper panels are average vertical velocity in clouds w_c, cloud area fraction σ, cloud mass flux M_c, average vertical velocity outside clouds w_{sub} and the radiative cooling R divided by the stability S. The lower panels show the same, but for convective regions (see main text for definition). All panels have the $y = x$ black, dotted curve for reference.

While w_{sub} broadly scales with R/S, we must note here that the magnitude of the two quantities do not show a very good match. As shown in Figure 9 in the Appendix, neither just a radiative balance nor a balance of radiative and re-evaporative cooling combined with subsidence warming lead to a good match, with the greatest mismatch occurring near the cloud anvil. This mismatch is briefly discussed in Appendix B. The fact that even the mid-tropospheric values do not match well indicate that looking at vertical velocities purely outside clouds is not a good measure for purely radiation driven subsidence. A cloud here is a point-wise metric requiring a threshold value of non-precipitating condensate mixing ratio and rising motion ($w > 0$). The mismatch is likely due to the large degree of turbulent vertical velocity fluctuations and strong return flows near the clouds which are related to the cloudy dynamics rather than subsidence in clear-sky regions far away from clouds.

Thus, we instead turn our attention to "convecting regions" – a vertical column is defined to be part of the convecting region if the column-intergrated cloud-water (CICW) is above a threshold of 0.5 kg m^{-2} (the results remain unchanged for a broad range of thresholds from 0.1 to 1 kg m^{-2}). The regions of high CICW are co-located with regions of high column-integrated precipitable water, high surface precipitation and high mid-tropospheric vertical velocity, indicating that these are regions of intense convective activity, even if momentarily they lack condensates at some height. Figure 9 in the Appendix shows that the average subsidence outside these regions matches closely with a pure radiative equilibrium. Thus, pure radiatively driven subsidence can be seen outside convecting regions rather than outside clouds alone.

The lower panels of Figure 3 show the scaling of average vertical velocity and the mass-flux within convecting regions as well as the area fraction occupied by these regions at the same temperature level as the upper panels (250 K). In other words, we performed the same analysis as above using the column-integrated threshold to identify convective regions instead of clouds identified by a point-wise metric. All these three quantities (shown in red) scale nearly identically in the upper and lower panels for VAT as well as CAT. This crucial fact indicates that across simulations, the clouds have very similar structures and, for instance, the ratio between the cloud fraction and the convecting area fraction remain fixed at a given temperature level.

The picture that emerges is that of rising, saturated cloud-plumes, with the area occupied by them expanding to increase their mass-flux while the dynamics within them are fairly constant. These cloud-plumes carry with them a region of intense activity which are not radiatively driven, instead driven simply by the dynamics close to them and phase changes of water which doesn't participate in the core of the cloud. This "cloud baggage" [1] also scales linearly with the cloud-plumes, so that when taken together, the cloud-plumes and their baggage form the convecting regions of the flow, responsible for clouds and precipitation. Outside these convecting regions, the dynamics is simply in balance with radiative cooling and directly feels the imprint of the varying R. The fact that the baggage is "well-behaved" is rather fortuitous, allowing the direct comparison of the vertical derivatives of R/S (or $(R + H_e)/S$) with the vertical derivative of w_{sub} measured outside clouds (Bony et al., 2016; Jeevanjee, 2022).

The invariance of w_c across simulations taken together with the linear scaling between the properties of the cloud-plumes and the cloud baggage suggests that the properties of the clouds, such as the area occupied by individual clouds, do not change much. Instead their numbers simply increase. Previous studies which varied R in similar CRM set-ups do find that the increase in cloudy area fraction is due to an increase in the number of clouds while the distribution of the sizes of the cloud-cores do not vary (Craig and Cohen, 2006; Cohen and Craig, 2006).

3.3 | Vertical Variation in Cloud Characteristics

To better understand the processes which set w in clouds, we assess the buoyancy within clouds. The lower panels of Figure 4 show the histogram of buoyancy at the 250 K level for the VAT and CAT simulation. We see here that the distribution of buoyancy does not show large differences, with even the tails of the distributions showing little difference in the CAT case. In the VAT case, the cases with larger R actually have smaller positive tails, consistent with the decrease in temperature and hence moisture and CAPE, leading to a smaller ability to create large positive buoyancies. This however is contrary to the observed small increase in w_c as well as extreme values of w with R.

The distribution of buoyancy at $z \sim 600$ m (top panels) on the other hand shows large differences with varying R. This height corresponds to the first height at which the average cloud fraction is above 0.1 % in all simulations, ensuring that the histogram is reasonably smooth. It corresponds to the 6th model level, which is close to the theoretical Lifted Condensation Level (LCL) for all the simulations (between the 5th and 6th levels). It is below the lower-tropospheric peak of cloud fraction in all but one simulation ($R = 0.75\,\mathrm{K\,d^{-1}}$), so it represents a regime at or just below the cloud-base level, where the dynamics is strongly influenced by the boundary layer. At this level, the buoyancy histogram shows sharp differences, with the positive and negative anomalies being much larger for the simulations with large R in both sets of simulations. With increasing R, the distribution also becomes flatter and the tails are more pronounced. The inset to the top right panel shows the vertical velocity within clouds at the same height, which we denote $w_c^{(b)}$. Here, unlike its mid-tropospheric counterpart, $w_c^{(b)}$ shows a noticeable increase with increasing R, showing a $\sim$ 3-fold increase in value in both sets of simulations.

The above discussion, while holding many insights into the scaling of moist convection still does not address

[1] We thank Prof. Robert Plant for suggesting this elegant terminology.

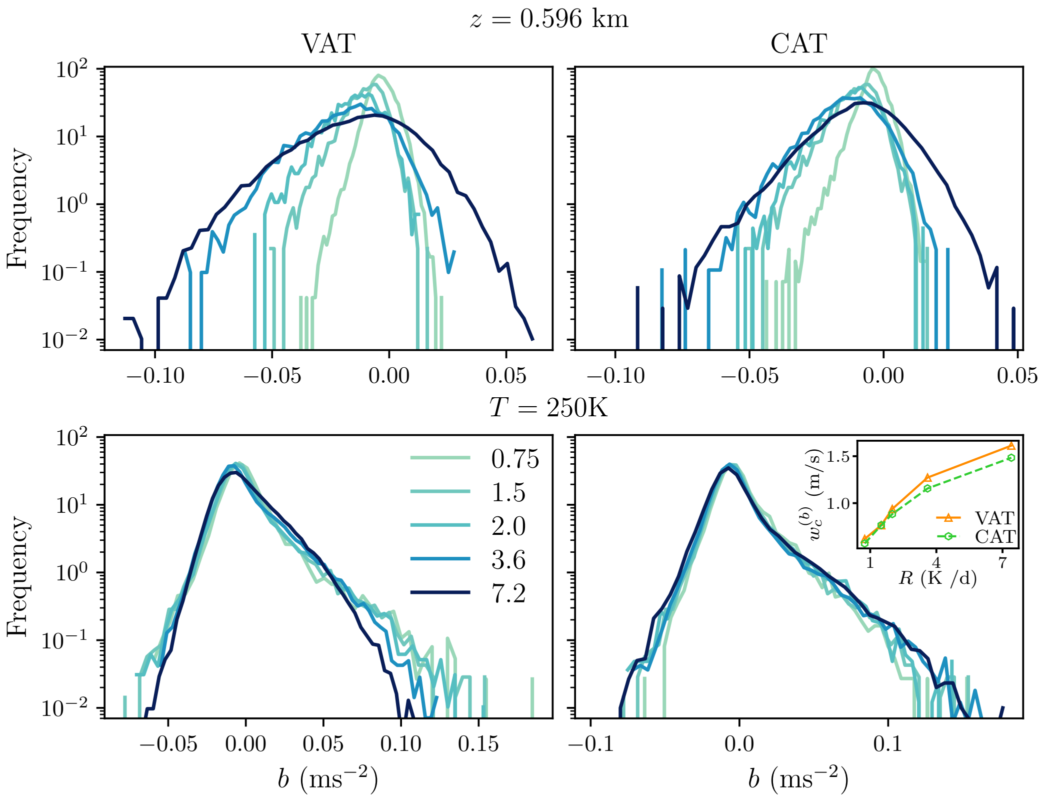

FIGURE 4 Histogram of the buoyancy in clouds in the boundary layer (z = 596 m - top panels) and temperature level closest to T = 250 K (lower panels) for the simulations with different R for VAT (left) and CAT (right). Inset in lower right panel shows the boundary layer vertical velocity $w_c^{(b)}$ at at the same height.

the vexing central question – why does the area alone expand rapidly with increasing R? Changing the radiative cooling impacts a host of different flow characteristics, including the surface fluxes, the domain mean temperature, the relative humidity and the stability. One set of quantities that remain remarkably constant across the simulations are the vertical variations in the various cloud characteristics considered in the preceding paragraphs. In particular, the vertical gradients in σ, w_c, M_c and w_{sub} plotted using temperature as a vertical coordinate follow almost exactly the same curves above the boundary layer in the mid- and upper-troposphere with large differences closer to the boundary. This is further discussed in Appendix A (see also Figure 8) and it shows that all these quantities have the same vertical structure and a common vertical form function, independent of the forcing. Any inter-simulation differences then must arise from differences which already exist at the top of the boundary layer.

Thus, instead of looking at the scaling of the velocity in clouds alone, in Figure 5 along with w_c, we plot various other quantities related to the vertical velocity. The 99.99-th percentile of vertical velocity is shown to scale similarly to w_c. w_{CAPE} is the prediction of w from the CAPE, that is the vertical integral of the buoyancy of a moist adiabatic parcel lifted from the surface up to the given temperature level. As stated earlier, CAPE decreases with R in both simulations. Finally, we show the scaling of w_c with the contribution of the top of boundary layer vertical velocity, or

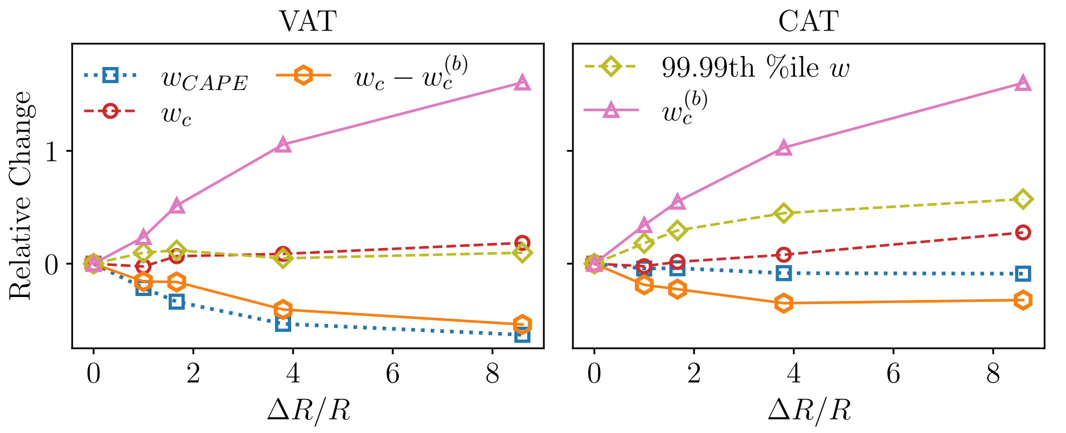

FIGURE 5 The relative change in various quantities plotted as a function of the relative change in R for varying air temperature and tuned air temperature simulations linearly interpolated to the $T = 250\,\mathrm{K}$ level. See main text for definitions.

$w_c^{(b)}$, removed. $w_c - w_c^{(b)}$ is thus a measure of the acceleration in the clouds above the boundary layer height, here taken to be 596 m. We have already seen in the inset of figure 4 that this value responds quite strongly to R. Here we see that the scaling of $w_c - w_c^{(b)}$ (green curve) closely follows the scaling of the prediction from CAPE (blue curve) in the VAT and CAT case. This scaling works similarly well for temperature levels below and close to the peak in the vertical profile of w_c. Above this level, the value of w_c starts to decrease while the moist-adiabat is still positively buoyant and it would be unphysical to continue to compare these curves. We note here that the peak in the extreme cloud velocities occur far higher up in the domain, closer to the 230 K temperature level and higher.

This shows that the apparent insensitivity of w_c to CAPE is actually a boundary effect. Even as the boundary becomes colder and drier, decreasing the moist instability and CAPE, the increasingly unstable boundary layer strongly driven by the stronger surface fluxes leads to large variability in the boundary layer, creating strongly accelerated, upward moving parcels at the cloud base itself. Above the cloud base, the on-average incremental upward acceleration is related to the more traditional instability measure of CAPE. The increased boundary layer variability is seen not only in the buoyancy distribution but also in the distributions of temperature, water vapour mixing ratio (and consequently, the moist static energy). We note that generally, plume-based models for predicting vertical velocities do not take into account large buoyancy or velocity anomalies arising within the boundary layer itself (Singh and O'Gorman, 2015). Our results thus suggest, at least within the idealised settings used here, that boundary layer dynamics might play a role in setting in-cloud velocities in addition to the acceleration from CAPE.

3.4 | A non-dimensional scaling for Moist Convection

In the appendix of AMC25, the authors suggested a non-dimensionalisation of the equations on the basis of setting the rate of radiative cooling to unity. This was done by setting temperature scale $\mathcal{T}$ and time-scale t_0 such that

$$R = \mathcal{T} t_0^{-1}. \tag{4}$$

Through this relation, setting either a time-scale automatically sets the temperature scale and vice-versa. This step is justified as in RCE, it is R that sets the dynamics of the entire system. As seen in this study, the dynamics also strongly depend on the surface temperature, which determines the availability of heat and moisture in the boundary layer. Increasing the SST for the same value of R increases w_c, decreases σ and M_c. The decrease of mass-flux with warming has been noted and can be seen within references of Jeevanjee (2022). One way to interpret this decrease is that a given rate of radiative cooling must be balanced by the transport of an equal amount of heat upward by convection. This heat is either transported directly, as sensible heat, or as latent heat by the transport of moisture. A warmer plume is also more moist, allowing the transport of more latent heat for the same mass of air, thus necessitating fewer plumes to balance the same amount of cooling.

AMC25 suggested the dimensionless parameter given by

$$\mathcal{N} = \frac{c_p R H}{q_0 U_0 L}, \tag{5}$$

where c_p is the specific heat-capacity of dry air, H is a vertical length scale, q_0 is a water-vapour mixing ratio scale, U_0 is a velocity scale and L is the latent heat of condensation of water. t_0 then is given by H/U_0, which gives the temperature scale from (4). In AMC25, U_0 was given by the diffusive velocity scale (Vallis et al., 2019) and H was simply the height of the domain. We notice here that the numerator of $\mathcal{N}$ is similar to a net cooling rate term for the entire height while the denominator is similar to a rate of latent heating. It can be seen that using $t_0 = H/U_0$ and $R = \mathcal{T}/t_0$ gives simply

$$\mathcal{N} = \frac{c_p \mathcal{T}}{L q_0}, \tag{6}$$

where $\mathcal{T}$ and q_0 are the appropriate temperature and water vapour mixing ratio scales.

We study the variation of $\mathcal{N}$ with the non-dimensionalised mass-flux, which we denote $\hat{M}_c$. We consider the height of the lower tropospheric peak in M_c as the cloud-base height, which lies above the LCL. Taking the same velocity scale U_0 and a density scale ρ_0 gives

$$\hat{M}_c = \frac{M_c|_{cb}}{\rho_0 U_0}, \tag{7}$$

where $M_c|_{cb}$ is the cloud mass-flux at this cloud-base height. The mass-flux at cloud-base is known to be closely related to the precipitation (Held and Soden, 2006; Jeevanjee, 2022), which is in turn equal to the LHF (modulo a constant related to ρ, c_p and the latent heat of condensation of water). Figure 6 shows $\hat{M}_c$ plotted against $\mathcal{N}$ in log-log coordinates. This is plotted for the VAT and CAT simulations (red squares) as well as an additional set of simulations (blue circles) where R and SST are varied widely using the same RCE set-up and details can be found in Appendix C.

Figure 6 shows $\mathcal{N}$ and $\hat{M}_c$ scale well with a simple $3/4$ power law. A linear-fit performed for the logarithm of the values yielded a slope of 0.783. In the inset of Figure 6, we show the log-log plot of the non-dimensionalised mass-flux with the same non-dimensional number $\mathcal{N}$ calculated for the 2D direct numerical simulations detailed in AMC25, discussed further in Appendix C. Here too, the response of the mass-flux scales closely with the same power-law when the imposed bulk cooling in the domain is varied by 1 order of magnitude. This indicates that the mass-flux in moist convection, similar to the Nusselt number of Rayleigh-Bénard convection (Heslot et al., 1987; Grossmann and Lohse, 2000) and numerous other non-dimensionalised flux metrics for various other forms of convection (Klinger and Marshall, 1995; Yang et al., 2016), follows a scaling power-law which is a constant in the regimes explored here.

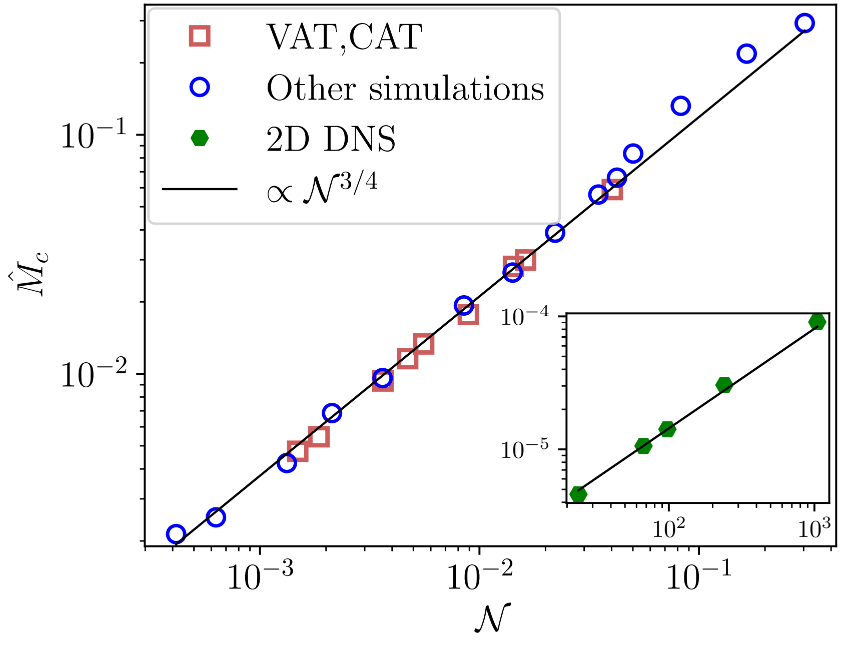

FIGURE 6 Log-log plot of non-dimensional parameter $\mathcal{N}$ versus the non-dimensionalised cloudy mass-flux $\hat{M}_c$ for the VAT, CAT simulations (red squares) and other simulations carried out with varying values of R and SST with the same set-up (see Table 2). Inset shows the same plot for the DNS simulations from AMC25.

This scaling can be rationalised and interpreted by considering that within the set-up of a typical RCE model with fixed radiative cooling as we have here, the dynamics is only a function of R and SST. When R increases, the difference in temperature between the surface (SST) and the first atmospheric level in the model (T_a) must increase so that the surface fluxes, parametrised by bulk formulae as proportional to this difference ΔT, also increase. The latent heat flux is also proportional to the difference Δq between the saturation mixing ratio at SST, $q^*(\mathrm{SST})$, and q_a. For a given SST, increasing R leads to a smaller q_a, leading to a larger increase (relative to the increase in R) in $\mathcal{N}$. This corresponds to the VAT simulations described in this study. On the other hand, if q_a is to be kept fixed as R is increased (decreased), then the SST must also be increased (decreased) accordingly. This corresponds to the CAT simulations described in this study.

Our empirical scaling suggests that for fixed q_a achieved by tuning the SST, $\hat{M}_c$ would scale roughly as $\sim R^{3/4}$, assuming small changes in U_0 and H. In case R is fixed and q_a alone is varied by varying the SST, then $\hat{M}_c$ would scale as $\sim q_a^{-3/4}$. This latter scaling is the observed decrease in cumulus mass-flux for a warmer atmosphere. In fact, under a global warming scenario with higher surface temperatures and increased atmospheric CO_2 concentration, q_a is expected to increase strongly ($\sim$ 7%/K) while the increase in total R in the troposphere is expected to be slower (Held and Soden, 2006), leading to a decrease in $\mathcal{N}$, again assuming that changes in H and U_0 are much smaller.

We make an informed guess that the scaling would break down at two different asymptotic regimes. Firstly, if R is held to be 0 but the SST is large enough, this would induce moist convection in the absence of the destabilisation by radiative cooling. This is the situation for example in Rainy-Bénard convection (Vallis et al., 2019) and other systems of simplified moist convection (Pauluis and Schumacher, 2010). Here, $\hat{M}_c$ is finite while $\mathcal{N}$ is 0. In the second scenario, in a system with large R in conjunction with small SST, the system would approach dry convection and there would be no “clouds" or significant moist dynamics – thus the quantity of mass-flux in clouds would be ill-defined. The behaviour of radiatively cooled, purely dry convection has been studied in Berlengiero et al. (2012); Agasthya and Muller (2024). Finally, we note that recently an alternate non-dimensional quantity to characterise the static stability of moist-convection with radiative cooling has been proposed by Dritschel et al. (2025) using CAPE calculated from the steady-state temperature profile which depends on molecular diffusivity of air as well as the rate of radiative cooling.

4 | CONCLUSION AND DISCUSSION

In this study, we have considered the cloud-resolving model SAM in an RCE configuration with constant sea surface temperature and with the radiative cooling idealised as a constant, bulk cooling term with rate R K d^{-1}. Our set-up and numerical experiments are very similar to previous work conducted in CRMs (Robe and Emanuel, 1996; Craig and Cohen, 2006) and DNS (Agasthya et al., 2025). We systematically vary R and study the response of the domain and various moist-convective parameters in the simulations, in particular the cloud mass-flux, the area fraction of the domain and the vertical velocity in clouds. To decouple the direct impact of varying R on the domain from the indirect effect of the changing temperature, we conduct an additional set of simulations where the SST is changed from simulation to simulation to achieve a nearly constant temperature profile across simulations.

We study the scaling of these convective parameters as a function of the imposed radiative cooling and find that, consistent with previous studies, the increase in cloud mass-flux M_c (an increase required for energy balance) occurs by an increase in cloud area fraction σ while the vertical velocity in clouds w_c shows only small changes. This scaling occurs in both, simulations with the same surface temperature (VAT) and simulations with the same atmospheric temperature (CAT), showing that the impact of the decrease in temperature of the domain is not important in causing an increase is convective area.

Outside clouds, the dynamics is set directly by radiative cooling, with the magnitude of subsiding velocity w_{sub} that increases according to a theoretical balance between subsidence warming and radiative-cooling as in (3). However, it is pertinent to note that while this scaling was found to hold outside clouds, w_{sub} defined this way is not quantitatively representative of radiative balance as it is an order of magnitude larger than the prediction from radiative cooling. Instead, we find that the dynamics outside “convecting regions" are more akin to a pure radiative balance.

We further find that the various cloud characteristics are functions of temperature alone, independent of any changes in large-scale circulation. This constrains the buoyancy within clouds to not grow large enough to produce large vertical velocities even when the surface fluxes are very large. The changes we do observe in vertical velocity can be explained by a combination of larger variability in the boundary layer with increasing R followed by vertical acceleration that broadly scales with CAPE above the boundary layer. The large variability in the boundary layer can be seen in the vertical velocity in clouds, where for simulations with larger R, cloud parcels have already acquired a significant vertical velocity even before they are accelerated by CAPE. The extreme vertical velocities are also found to scale with R similar to the average in-cloud vertical velocities.

Finally, we use a non-dimensionalisation suggested previously in AMC25 to propose a scaling for moist convection which holds true for cloud resolving model simulations as well as direct numerical simulations. The non-dimensionalised mass-flux $\hat{M}_c$ scales as $\mathcal{N}^{3/4}$, where $\mathcal{N}$ is the non-dimensionalised ratio between the rate of radiative cooling R and the water-vapour mixing ratio at the surface q_a. The temperature scale is set by considering R to be of magnitude unity while the length and velocity scales are set to be the vertical extent of moist-convection in the domain and the vertical velocity in clouds respectively. It remains to be seen to what extent the non-dimensional scaling discovered here is generally applicable to moist convection, particularly in the case where radiative cooling is not fixed externally but is represented realistically. Initial results from RCE simulations performed with fixed SST, fully interactive radiation and changing CO_2 by the authors indicate that the $3/4$ power-law relationship also holds in this case, though the parameter space explored was fairly narrow.

A key aspect that needs further investigation is the scope and relevance of the current study. It remains to understand if the slow change in vertical velocity and strong response of cloud area to varying large-scale forcing studied and characterised here should be interpreted as a tropics-wide change in RCE or can also be seen over smaller time and length scales. The applicability of RCE simulation results to the Earth's atmosphere has been vigorously debated (Singh and O'Gorman, 2013; Seeley and Romps, 2015; Romps, 2021) and the results here are not immune from this debate. This gap could be bridged by assessing global climate model outputs, particularly storm-resolving models (Stevens et al., 2019) which resolve deep convection without parametrisations. Non-equilibrium studies of limited-domain models of moist convection are also a candidate to shed light further on this topic. An interesting question to ask is – under what model conditions could few clouds with large w_c be generated as a response to increasing R?

In this study, we have taken a step in moving towards unifying studies on highly idealised prototypes of convection with more realistic models. This family of models ranges from classical Rayleigh-Bénard convection to realistic regional and global climate models, with various degrees of idealisations, simplifications and parametrisations in between. Fundamental studies of moist convection and general convection hold several insights into the behaviour of the earth's atmosphere, whether for dry convection, shallow moist convection or deep moist convection.

Acknowledgements

The authors gratefully acknowledge discussions with Prof. Robert Plant (University of Reading, United Kingdom), Prof. Steve Tobias, Prof. Douglas Parker and Gregory Dritschel (University of Leeds, United Kingdom). Discussions with colleagues at The Institute of Science and Technology Austria played a large role in shaping this study. The authors are particularly grateful for the inputs and discussions from Dr. Jiawei Bao, Dr. Alejandro Casallas and Alzbeta Pechacova.

This project has received funding from the European Union's Horizon 2020 research and innovation programme under the Marie Sklodowska-Curie grant agreement No. 101034413. CM gratefully acknowledges funding from the European Research Council (ERC) under the European Union's Horizon 2020 research and innovation program (Project CLUSTER, Grant Agreement No. 805041). This research was supported by the Scientific Service Units (SSU) of IST Austria through resources provided by Scientific Computing (SciComp).

conflict of interest

The authors report no conflict of interest.

Data Availability Statement

The data that support the findings of this study are available from the corresponding author, Lokahith Agasthya, upon reasonable request.

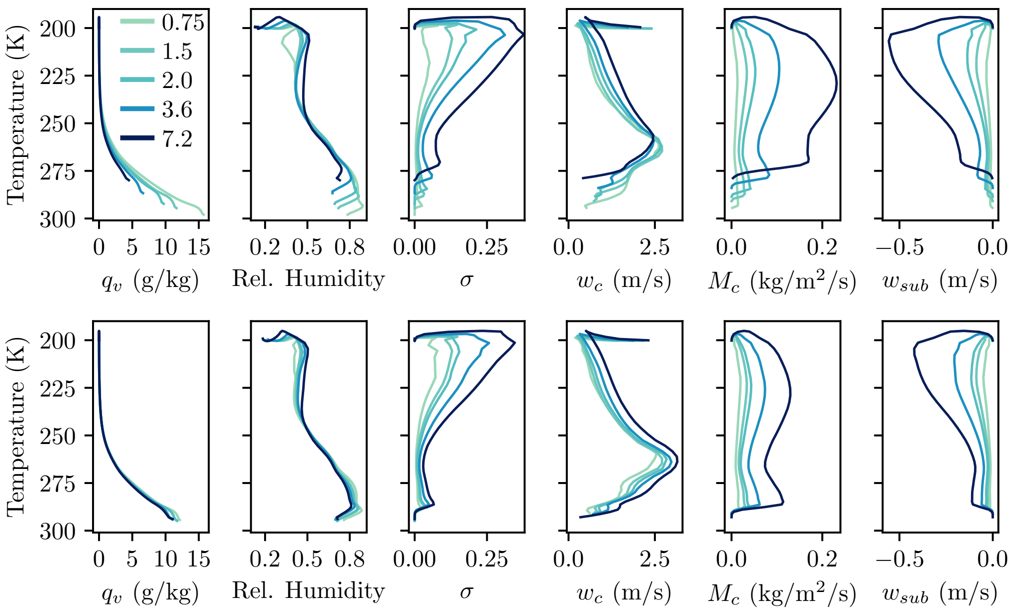

FIGURE 7 (From left to right) Time and horizontally averaged profiles of water vapour mixing ratio q_v, relative humidity, cloud area fraction σ, vertical velocity in clouds w_c, cloud mass flux M_c and vertical velocity outside clouds w_{sub} for VAT simulations (top panels) and CAT simulations (bottom panels). The profiles are plotted against the averaged temperature profile, ie., on isothermal coordinates.

A | ISOTHERMAL COORDINATES

The scaling of moist convective and other quantities are plotted at fixed temperature levels rather than a fixed height at various points in the main text. Previous studies (Robe and Emanuel, 1996) compared w_c, σ and M_c at the same height. However, this captures different convective dynamics in different simulations. In Figure 7, we plot the profiles from Figures 1 and 2 in isothermal coordinates, that is, using the average temperature profile as the vertical coordinate. We note several features of interest. Firstly, despite very different conditions in the sub-cloud layer in the VAT simulations, all the profiles of relative humidity are nearly invariant with temperature across simulations in the mid-troposphere. The basic physics behind this RH-T invariance has been studied before (Romps, 2014).

The cloud-base can be discerned by looking at the lower tropospheric maximum of the cloud area fraction (which is the same as the maximum in M_c). For the VAT simulations, this cloud-base occurs at very different temperatures. However, the mid-tropospheric peaks in w_c are much closer together, slightly shifting upward for larger R. The upper peak in σ which closely corresponds to the minimum of w_{sub} is the cloud anvil and this too occurs at a roughly fixed temperature, independent of the lower tropospheric temperature. This is however expected, given that we enforce a fixed stratospheric temperature of 200 K. We choose a temperature level close to 250 K for our analysis as this is close to the peak of w_c and is in a regime where the cloud area is increasing with height, influenced purely by in-cloud processes.

In the CAT simulations, due to the temperature profiles being nearly identical, all the curves have the same shape

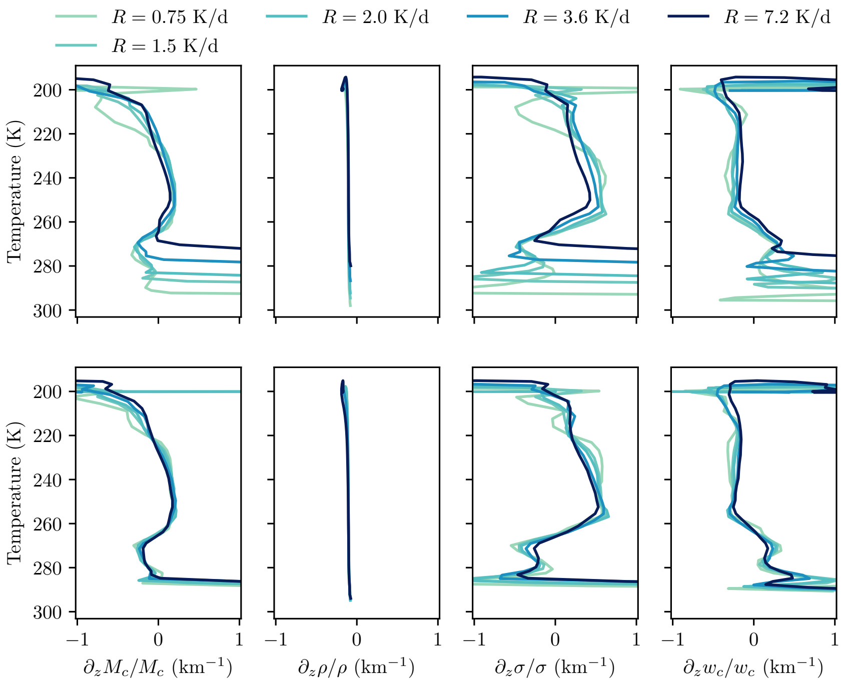

FIGURE 8 Plots showing the fractional rate of vertical change for M_c, ρ, σ, w_c for VAT (upper panels) and CAT (lower panels) plotted on isothermal coordinates.

in the vertical when plotted in isothermal coordinates as when they are plotted as a function of height.

In addition to the quantities themselves, in Figure 8, we study the vertical variation in the mass-flux and the three quantities that make up the mass-flux. We find again in the mid-troposphere above the boundary layer, the vertical derivative in these quantities are a function of temperature alone across simulations, as alluded to in § 3.3.

B | SUBSIDENCE VELOCITY

Figure 9 shows the average subsidence velocity w_{sub} outside clouds. It is seen here that there is a large mismatch between this value (blue) and the prediction from a pure radiative balance (green, dashed curve). This match does not improve greatly when the cooling due to the re-evaporation of falling rain is also included (dotted, brown curve) in the prediction, as suggested by Jeevanjee (2022). The mismatch is especially large near the cloud anvil – here convergence outside clouds is known to play a stronger role in producing subsidence velocities. However, we found that including the horizontal convergence term still does not improve the prediction (not shown), indicating that non steady-state forces also play an important role in the convective dynamics. A deeper investigation into this is beyond the scope of the current study. Here we simply note that better quantitative agreement is obtained when we compute subsidence velocity $w_{sub}^{(conv)}$ outside convective regions defined with a CICW threshold (see § 3.2 for details).

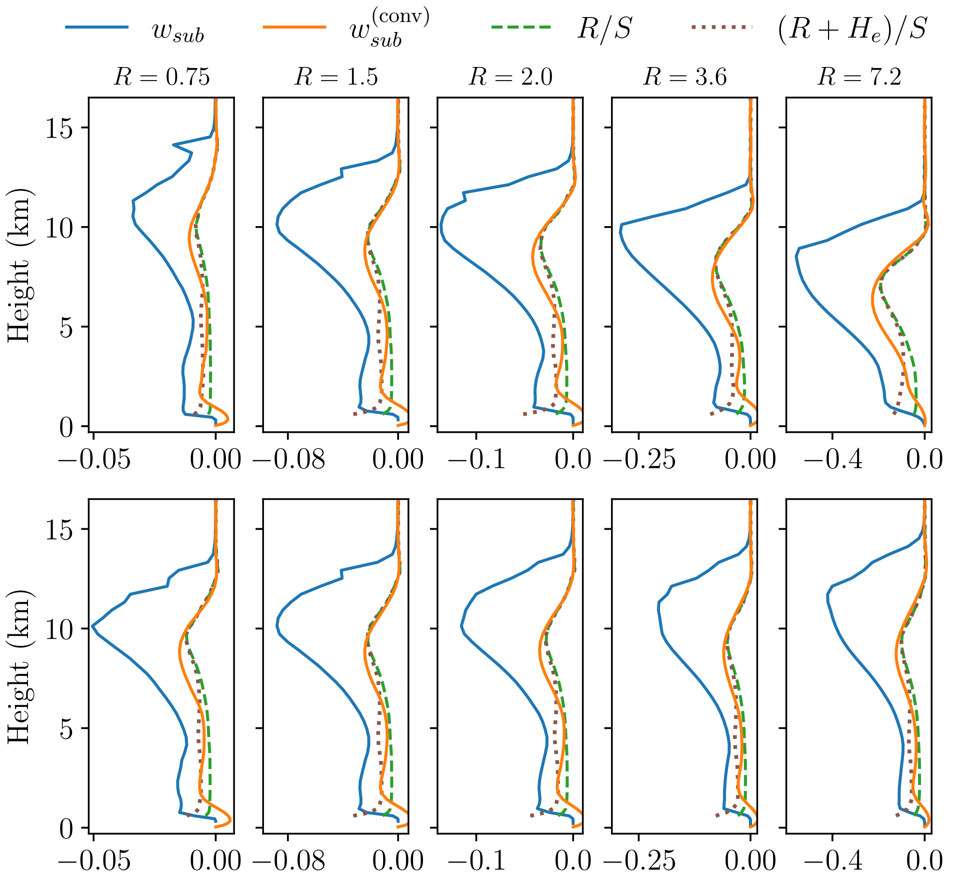

FIGURE 9 Time and horizontally averaged profiles of vertical velocity in m s^{-1} outside clouds (solid blue curve), outside convective regions (solid orange curve) compared with the prediction of pure radiative balance R/S (dashed green curve) and a radiation + reevaporation balance (dotted brown curve) in VAT simulations (top panels) and CAT simulations (bottom panels) for all the studied values of R in K d^{-1} as indicated by the plot titles. Note that the x-axes ranges vary for different R.

C | NON-DIMENSIONAL SCALING

In addition to the VAT and CAT simulations, we performed RCE simulations with fixed radiative cooling R and constant SST across a wider range of parameters to understand the scaling of the non-dimensional parameters $\mathcal{N}$ and $\hat{M}_c$ introduced in § 3.4. The values of R and SST chosen are listed in Table 2.

For the DNS simulations of moist convection, the velocity scale was chosen as the usual diffusive velocity as given in AMC25, while the length-scale was simply the height of the domain. For q_0, the water vapour mixing ratio at $z = 1$ was chosen while for $\hat{M}_c$, the mass-flux was assessed at $z = 5$ in the simulation units of their study. For q_a, $z = 1$ corresponded a height above the diffusive boundary in all the simulations. The peak of M_c was close to $z = 5$, since the DNS simulations were performed assuming constant density (Boussinesq approximation) rather than decreasing

$R\,(\mathrm{K\,d^{-1}})$	SST (K)
0.5	(295, 305, 310)
2	(295, 305, 310)
6	(295, 305, 310)
10	(290,295, 305, 310)

TABLE 2 List of parameters R and SST for which additional simulations with the same set-up were performed to obtain the points in Figure 6.

with height.

references

Agasthya, L., Muller, C. and Cheve, M. (2025) Moist convective scaling: Insights from an idealised model. *Quarterly Journal of the Royal Meteorological Society*, **151**, e4902. URL: https://rmets.onlinelibrary.wiley.com/doi/abs/10.1002/qj.4902.

Agasthya, L. and Muller, C. J. (2024) Dynamics and scaling of internally cooled convection. *Communications in Nonlinear Science and Numerical Simulation*, **134**, 108011.

Arakawa, A. and Schubert, W. H. (1974) Interaction of a cumulus cloud ensemble with the large-scale environment, part i. *Journal of the atmospheric sciences*, **31**, 674–701.

Arakawa, A. and Wu, C.-M. (2013) A unified representation of deep moist convection in numerical modeling of the atmosphere. part i. *Journal of the Atmospheric Sciences*, **70**, 1977–1992.

Berlengiero, M., Emanuel, K., Von Hardenberg, J., Provenzale, A. and Spiegel, E. (2012) Internally cooled convection: a fillip for philip. *Communications in Nonlinear Science and Numerical Simulation*, **17**, 1998–2007.

Bony, S., Stevens, B., Coppin, D., Becker, T., Reed, K. A., Voigt, A. and Medeiros, B. (2016) Thermodynamic control of anvil cloud amount. *Proceedings of the National Academy of Sciences*, **113**, 8927–8932.

Bretherton, C. S., Blossey, P. N. and Khairoutdinov, M. (2005) An energy-balance analysis of deep convective self-aggregation above uniform sst. *Journal of the atmospheric sciences*, **62**, 4273–4292.

Cohen, B. G. and Craig, G. C. (2006) Fluctuations in an equilibrium convective ensemble. part ii: Numerical experiments. *Journal of the atmospheric sciences*, **63**, 2005–2015.

Craig, G. C. and Cohen, B. G. (2006) Fluctuations in an equilibrium convective ensemble. part i: Theoretical formulation. *Journal of the atmospheric sciences*, **63**, 1996–2004.

Dritschel, G. N., Tobias, S. M., Parker, D. J. and Tomassini, L. (2025) Radiatively-cooled moist convection under an idealised climate change scenario: Linear analysis. *arXiv preprint arXiv:2504.06019*.

Emanuel, K. A. (1994) *Atmospheric convection*. Oxford University Press, USA.

Grossmann, S. and Lohse, D. (2000) Scaling in thermal convection: a unifying theory. *Journal of Fluid Mechanics*, **407**, 27–56.

Held, I. M. and Soden, B. J. (2006) Robust responses of the hydrological cycle to global warming. *Journal of climate*, **19**, 5686–5699.

Heslot, F., Castaing, B. and Libchaber, A. (1987) Transitions to turbulence in helium gas. *Physical Review A*, **36**, 5870.

Holloway, C. E., Wing, A. A., Bony, S., Muller, C., Masunaga, H., L'Ecuyer, T. S., Turner, D. D. and Zuidema, P. (2017) Observing convective aggregation. *Surveys in Geophysics*, **38**, 1199–1236.

Houze Jr., R. A. (2004) Mesoscale convective systems. *Reviews of Geophysics*, **42**. URL: https://agupubs.onlinelibrary.wiley.com/doi/abs/10.1029/2004RG000150.

Jakob, C., Singh, M. and Jungandreas, L. (2019) Radiative convective equilibrium and organized convection: An observational perspective. *Journal of Geophysical Research: Atmospheres*, **124**, 5418–5430.

Jeevanjee, N. (2022) Three rules for the decrease of tropical convection with global warming. *Journal of Advances in Modeling Earth Systems*, **14**, e2022MS003285.

Jeevanjee, N. and Fueglistaler, S. (2020) Simple spectral models for atmospheric radiative cooling. *Journal of the Atmospheric Sciences*, **77**, 479–497.

Johns, R. H. and Doswell III, C. A. (1992) Severe local storms forecasting. *Weather and Forecasting*, **7**, 588–612.

Khairoutdinov, M. F. and Randall, D. A. (2003) Cloud resolving modeling of the arm summer 1997 iop: Model formulation, results, uncertainties, and sensitivities. *Journal of the Atmospheric Sciences*, **60**, 607–625.

Kiladis, G. N., Wheeler, M. C., Haertel, P. T., Straub, K. H. and Roundy, P. E. (2009) Convectively coupled equatorial waves. *Reviews of Geophysics*, **47**. URL: https://agupubs.onlinelibrary.wiley.com/doi/abs/10.1029/2008RG000266.

Klinger, B. A. and Marshall, J. (1995) Regimes and scaling laws for rotating deep convection in the ocean. *Dynamics of atmospheres and oceans*, **21**, 227–256.

Manabe, S. and Strickler, R. F. (1964) Thermal equilibrium of the atmosphere with a convective adjustment. *Journal of the Atmospheric Sciences*, **21**, 361–385.

Muller, C. J. and Held, I. M. (2012) Detailed investigation of the self-aggregation of convection in cloud-resolving simulations. *Journal of the Atmospheric Sciences*, **69**, 2551–2565.

Muller, C. J. and O'Gorman, P. (2011) An energetic perspective on the regional response of precipitation to climate change. *Nature Climate Change*, **1**, 266–271.

Muller, C. J., O'Gorman, P. A. and Back, L. E. (2011) Intensification of precipitation extremes with warming in a cloud-resolving model. *Journal of Climate*, **24**, 2784–2800.

Parodi, A. and Emanuel, K. (2009) A theory for buoyancy and velocity scales in deep moist convection. *Journal of the Atmospheric Sciences*, **66**, 3449–3463.

Pauluis, O. and Garner, S. (2006) Sensitivity of radiative–convective equilibrium simulations to horizontal resolution. *Journal of the atmospheric sciences*, **63**, 1910–1923.

Pauluis, O. and Schumacher, J. (2010) Idealized moist rayleigh-bénard convection with piecewise linear equation of state. *Communications in Mathematical Sciences*, **8**, 295–319.

Rayleigh, L. (1916) Lix. on convection currents in a horizontal layer of fluid, when the higher temperature is on the under side. *The London, Edinburgh, and Dublin Philosophical Magazine and Journal of Science*, **32**, 529–546.

Robe, F. R. and Emanuel, K. A. (1996) Moist convective scaling: Some inferences from three-dimensional cloud ensemble simulations. *Journal of Atmospheric Sciences*, **53**, 3265–3275.

Romps, D. M. (2014) An analytical model for tropical relative humidity. *Journal of Climate*, **27**, 7432–7449.

— (2021) Ascending columns, wtg, and convective aggregation. *Journal of the Atmospheric Sciences*, **78**, 497–508.

Seeley, J. T. and Romps, D. M. (2015) Why does tropical convective available potential energy (cape) increase with warming? *Geophysical Research Letters*, **42**, 10–429.

Shutts, G. and Gray, M. (1999) Numerical simulations of convective equilibrium under prescribed forcing. *Quarterly Journal of the Royal Meteorological Society*, **125**, 2767–2787.

Singh, M. S. and Neogi, S. (2022) On the interaction between moist convection and large-scale ascent in the tropics. *Journal of Climate*, **35**, 4417–4435.

Singh, M. S. and O'Gorman, P. A. (2013) Influence of entrainment on the thermal stratification in simulations of radiative-convective equilibrium. *Geophysical Research Letters*, **40**, 4398–4403.

— (2015) Increases in moist-convective updraught velocities with warming in radiative-convective equilibrium. *Quarterly Journal of the Royal Meteorological Society*, **141**, 2828–2838. URL: https://rmets.onlinelibrary.wiley.com/doi/abs/10.1002/qj.2567.

Singh, M. S. and O'Gorman, P. A. (2012) Upward shift of the atmospheric general circulation under global warming: Theory and simulations. *Journal of Climate*, **25**, 8259–8276.

Stauffer, C. L. and Wing, A. A. (2022) Properties, changes, and controls of deep-convecting clouds in radiative-convective equilibrium. *Journal of Advances in Modeling Earth Systems*, **14**, e2021MS002917. URL: https://agupubs.onlinelibrary.wiley.com/doi/abs/10.1029/2021MS002917. E2021MS002917 2021MS002917.

Stevens, B. (2005) Atmospheric moist convection. *Annual Review of Earth and Planetary Sciences*, **33**, 605–643. URL: https://www.annualreviews.org/content/journals/10.1146/annurev.earth.33.092203.122658.

Stevens, B., Satoh, M., Auger, L., Biercamp, J., Bretherton, C. S., Chen, X., Düben, P., Judt, F., Khairoutdinov, M., Klocke, D. et al. (2019) Dyamond: the dynamics of the atmospheric general circulation modeled on non-hydrostatic domains. *Progress in Earth and Planetary Science*, **6**, 1–17.

Tompkins, A. M. and Craig, G. C. (1998) Radiative–convective equilibrium in a three-dimensional cloud-ensemble model. *Quarterly Journal of the Royal Meteorological Society*, **124**, 2073–2097.

Vallis, G. K., Parker, D. J. and Tobias, S. M. (2019) A simple system for moist convection: the rainy–bénard model. *Journal of Fluid Mechanics*, **862**, 162–199.

Wing, A. A., Emanuel, K., Holloway, C. E. and Muller, C. (2017) Convective self-aggregation in numerical simulations: A review. *Shallow clouds, water vapor, circulation, and climate sensitivity*, 1–25.

Wing, A. A. and Emanuel, K. A. (2014) Physical mechanisms controlling self-aggregation of convection in idealized numerical modeling simulations. *Journal of Advances in Modeling Earth Systems*, **6**, 59–74. URL: https://agupubs.onlinelibrary.wiley.com/doi/abs/10.1002/2013MS000269.

Yang, Y., Verzicco, R. and Lohse, D. (2016) Scaling laws and flow structures of double diffusive convection in the finger regime. *Journal of Fluid Mechanics*, **802**, 667–689.

Yano, J.-I. and Plant, R. (2012) Finite departure from convective quasi-equilibrium: Periodic cycle and discharge–recharge mechanism. *Quarterly Journal of the Royal Meteorological Society*, **138**, 626–637.

Zhang, C. (2005) Madden-julian oscillation. *Reviews of Geophysics*, **43**. URL: https://agupubs.onlinelibrary.wiley.com/doi/abs/10.1029/2004RG000158.